ACS APPLIED MATERIALS & INTERFACES

Research Article

www.acsami.org

Graft Copolymer Nanoparticles with pH and Reduction Dual-Induced Disassemblable Property for Enhanced Intracellular Curcumin Release

Junqiang Zhao,[†,‡,§] Jinjian Liu,[†,⊥] Shuxin Xu,[§] Junhui Zhou,[§] Shangcong Han,[§] Liandong Deng,[§] Jianhua Zhang,[§] Jianfeng Liu,[⊥] Aimin Meng,[⊥] and Anjie Dong*[,‡,§,#]

[‡]School of Materials Science and Engineering, Tianjin University, Tianjin 300072, P.R. China

[§]Department of Polymer Science and Technology and Key Laboratory of Systems Bioengineering of the Ministry of Education, School of Chemical Engineering and Technology, Tianjin University, Tianjin 300072, P.R. China

[⊥]Tianjin Key Laboratory of Molecular Nuclear Medicine, Institute of Radiation Medicine, Chinese Academy of Medical Science and Peking Union Medical College, Tianjin 300192, P.R. China

[#]Collaborative Innovation Center of Chemical Science and Engineering (Tianjin), Tianjin 300072, P.R. China

ABSTRACT: Nanoparticle (NP)-assisted drug delivery systems with disassemblable behaviors in response to intracellular microenvironment are urgently demanded in systemic cancer chemotherapy for enhanced intracellular drug release. Curcumin (CUR), an effective and safe anticancer agent, was limited by its water insolubility and poor bioavailability. Herein, pH and reduction dual-induced disassemblable NPs for high loading efficiency and improved intracellular release of CUR were developed based on an acid degradable cyclic benzylidene acetal groups (CBAs)-functionalized poly(2,4,6-trimethoxybenzylidene-1,1,1-tris(hydroxymethyl)ethane methacrylate)-*g*-SS-poly(ethylene glycol) (PTTMA-*g*-SS-PEG) graft copolymer, which was readily prepared via RAFT copolymerization and coupling reaction. The NPs self-assembled from PTTMA-*g*-SS-PEG copolymers were stable at physiological pH, and quickly disassembled in mildly acidic and reductive environments because of the hydrolysis of CBAs in hydrophobic PTTMA core and the cleavage of disulfide-linked detachable PEG shell. PTTMA-*g*-SS-PEG NPs exhibited excellent CUR loading capacity with drug loading content up to 19.2% and entrapment efficiency of 96.0%. Within 20 h in vitro, less than 15.0% of CUR was released from the CUR-loaded NPs in normal physiological conditions, whereas 94.3% was released in the presence of reductive agent and mildly acidic conditions analogous to the microenvironment in endosome/lysosome and cytoplasm. Confocal fluorescence microscopies revealed that the CUR-loaded PTTMA-*g*-SS-PEG NPs exhibited more efficiently intracellular CUR release for EC-109 cells than that of CUR-loaded reduction-unresponsive PTTMA-*g*-PEG NPs and free CUR. In vitro cytotoxicity studies displayed blank PTTMA-*g*-SS-PEG NPs showed low toxicity at concentrations up to 1.0 mg/mL, whereas CUR-loaded PTTMA-*g*-SS-PEG NPs demonstrated more efficient growth inhibition toward EC-109 and HepG-2 cells than reduction-unresponsive controls and free CUR. Therefore, the above results indicated that pH and reduction dual-induced disassemblable PTTMA-*g*-SS-PEG NPs may have emerged as superior nanocarriers for active loading and promoted intracellular drug delivery in systemic cancer chemotherapy.

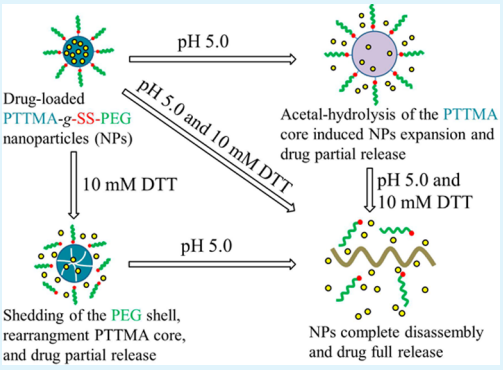

KEYWORDS: *cyclic benzylidene acetal, graft copolymer nanoparticle, pH and reduction dual-responsive, disassembly, curcumin*

INTRODUCTION

Over the last few decades, various environment-sensitive polymeric nanoparticles (NPs) have been developed as potential nanocarriers for tumor-targeted and controlled delivery of anticancer drugs to overcome their limitations like low therapeutic efficacy and intolerable side effects.[1−3] pH and reduction dual-sensitive NPs are the most widely used stimuli-responsive drug carriers for improving intracellular anticancer drug delivery.[4−7] On the one hand, the microenvironment in tumor tissues is more acidic (0.5−1.0 pH units lower) than in the normal tissues. And it is more remarkable that a prominent pH shift takes place during cellular uptake of NPs from blood or extracellular spaces (pH 7.2−7.4) to the various intracellular compartments (pH 4.0−6.5).[8,9] On the other hand, The concentration of glutathione (g-glutamyl-cys-teinyl-glycine; GSH), the most abundant thiol-containing peptide in animal cells, is very low (about 2−20 μM) in the cellular exterior, but much higher (0.5−10 mM) in the cytoplasm. Furthermore, there exists about 4-fold higher concentration of GSH in tumor tissues than the normal tissues.[10−13] Beyond that, the protein

Received: September 26, 2013
Accepted: December 6, 2013
Published: December 6, 2013

Scheme 1. Schematic Illustration of the Self-Assembly of the Drug-Loaded PTTMA-*g*-SS-PEG Graft Copolymer NPs and Their Disassembly Process Induced by pH and Reduction for Dually Triggered Release of Anticancer Drug

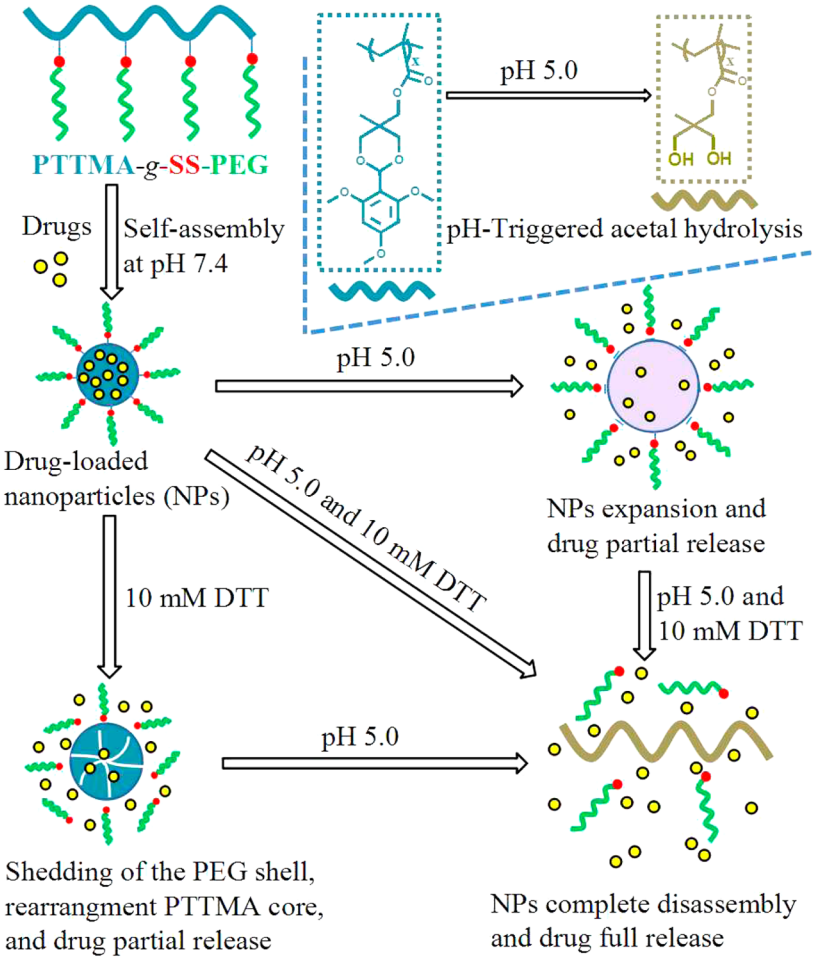

disulfide isomerase contained in plasma membrane, the cell membranes-associated NADH-oxidase, and redox enzymes in cytoplasm are all exhibiting disulfide-thiol interchange activity.[14]

By now, many kinds of pH and redox dual-sensitive nanocarriers had been designed and prepared for intracellular anticancer drug delivery, such as PEG-SS-PDEA polymersomes,[15] PMAA-based nanogels,[16] PEG-SS-PTMBPEC micelles,[17] mPEG-PAsp(MEA)-PAsp(DIP) micelles,[7] PDPA/PMAA-based capsules,[18] and so on. However, combining the high drug loading efficiency, minimal drug release in normal physiological conditions, quick disassembly under intracellular conditions, as well as convenient fabrication, was still the important issue to be addressed in developing anticancer drug nanocarriers.[6] For example, the complex and uncontrollable preparation of the pH and redox dual-sensitive based capsules or nanogels were not convenient to load anticancer drug and store.[16,18] The weak stability of polymeric micelles due to the strong shear stress and dilution action in blood circulation in vivo would result in premature release and drug loss and thereafter severe side effects.[19] It has been known that the nano aggregates self-assembled from graft copolymers exhibited excellent stability derived from low critical micelle concentration (CMC), functional adjustability both for the core and surface facilely by controlling the length of backbone, the density and length of graft side chains, as well as combining of variable density functional ligands into hydrophilic grafts for optimal tumor targeting.[20−22] Nevertheless, very little research has been focused on pH and redox dual-sensitive nanocarriers based on graft copolymeric amphiphiles.

Recently, pendent cyclic benzylidene acetal groups (CBAs) functionalized hydrophobic cores of polymeric nano aggregates have been considered as an effective strategy, because of the fact that the acetal groups are acid-labile and therefore can be hydrolyzed during intracellular mildly acidic environments. Moreover, most hydrophobic drugs contain aromatic or cyclic rings. The aromatic groups as the hydrophobic moiety would cause strong $\pi-\pi$ interactions with the drug molecules, which are beneficial for a higher drug encapsulation. Very recently, CBA-functionalized supramolecular assemblies,[23] micelles,[24,25] polymersomes,[26] cross-linked NPs[19,27] have emerged as potential vehicles for the specifically delivery of the therapeutic cargo inside cells.

Curcumin (CUR), a kind of curcuma longa rhizome-extracted natural chemotherapeutic agent, is an important alternative for cancer therapy as a potent modulator of inflammatory cell signaling, which regulates cell proliferation, apoptosis, and invasion.[28,29] Two major limits of CUR are its low solubility in water (0.4 μg/mL at pH 7.4) and degradation at physiological pH, resulting in a low bioavailability of CUR. Therefore, it is of vital importance to efficiently transport CUR into the tumor cell to exert its anticancer activity.[30,31]

Herein, pH and reduction dual-induced disassemblable NPs of graft copolymer, PTTMA-*g*-SS-PEG, was controlled synthesized by RAFT copolymerization and coupling reaction. As shown in Scheme 1, the CBAs functionalized hydrophobic cores formed by PTTMA would provide acid-labile disassemblable function to the drug-loaded NPs, and the reductive degradable disulfide bonds would give detachability of the PEG shell, which may further enhance the disassembly of PTTMA-*g*-SS-PEG NPs. The self-assembly and pH/reduction dual-induced disassembly behaviors of this novel graft copolymer NPs were investigated in detail. At the same time, loading and in vitro release of CUR, and cellular proliferation inhibition of CUR-loaded PTTMA-*g*-SS-PEG NPs were also investigated.

MATERIALS AND METHODS

Materials. 2,4,6-Trimethoxybenzylidene-1,1,1-tris-(hydroxymethyl)ethane methacrylate (TTMA) was synthesized via aldol condensation and esterification reaction by our lab according to the previously literature procedure.[27] Methoxy poly(ethylene glycol) (PEG, M_n = 2.0 kDa, PDI = 1.03) provided by Fluka was used after drying by azeotropic distillation from anhydrous toluene. Dicyclohexyl carbodiimide (DCC, 99%), 4-dimethylaminopyridine (DMAP, 99%), N-hydroxysuccinimide (NHS, 98%), N-(3-dimethylaminopropyl)-N′-ethylcarbodiimide hydrochloride (EDC, 99%), cystamine dihydrochloride (cystamine·2HCl, 98%), *p*-nitrophenyl chloroformate (97%,), 1,4-dithio-DL-threitol (DTT, 99%), methacrylic acid (MAA, 99%), azobisisobutyronitrile (AIBN, 99%), and curcumin (CUR, 98%) were purchased from Alfa Aesar. Dichloromethane, dimethyl sulfoxide (DMSO), ethyl acetate, triethylamine (Et_3N), diethyl ether, toluene, tetrahydrofuran (THF), and anhydrous sodium sulfate were provided by Jiangtian Co. (Tianjin, China). MAA was used after reduced pressure distillation. AIBN was recrystallized twice from methanol. 2-Cyanopropan-2-yl dodecyl trithiocarbonate (CPDTC) was obtained by our lab according to the previously literature procedure.[32]

Synthesis of Amphiphilic PTTMA-*g*-SS-PEG Graft Copolymer. PTTMA-*g*-SS-PEG was synthesized (Scheme 2) by combining RAFT copolymerization and coupling reaction.

Synthesis of P(TTMA-co-MAA). P(TTMA-*co*-MAA) copolymer was prepared via RAFT copolymerization of MAA and TTMA using CPDTC as a RAFT chain transfer agent. Briefly, MAA (72 mg, 0.84 mmol), TTMA (0.91 g, 2.47 mmol), CPDTC (25.0 mg, 0.10 mmol), AIBN (3.28 mg, 0.02 mmol), and toluene (4.0 mL) were mixed in a 10 mL Schlenk flask. After degassing via three freeze−pump−thaw cycles, the flask was placed in a thermostatic oil bath at 65 °C for 24 h under a N_2 atmosphere. And then P(TTMA-*co*-MAA) copolymer was collected into an excess of cold diethyl ether and dried in vacuo at 25 °C for 48 h. Yield: 94.2%. M_n (GPC) = 9.6 kDa, M_n (^{1}H-NMR) = 9.85 kDa, M_w/M_n(GPC) = 1.23. FT-IR (KBr): ν(cm^{-1}) 2945, 738, and 666 (aromatic -C-H), 2840 and 1367 (methylic −C-H), 1726 (carbonyl −C═O), 1605 (aromatic −C-C-), 1465 (methylene −C-H), and 1030 (-O-CH_3). ^{1}H-NMR ($CDCl_3$): δ 6.05 (aromatic protons), 5.89 (Ar-CH-), 3.89 (-OCH_2CCH_2O-), 3.75 (Ar-OCH_3), 1.85 ((CH_3)$_2$C-, -CH_2CCH_2-), 1.22 (-$(CH_2)_{10}$-), 0.50−1.15 (CH_3CCOO-, CH_3C-).

Synthesis of Cystamine-Functionalized PEG (PEG-SS-NH$_2$). PEG-SS-NH_2 was synthesized according to the previously reported literature.[33] Typically, the DMSO (15 mL) solution containing Et_3N (5.0 g, 50 mmol) and cystamine·2HCl (4.5 g, 20 mmol) was dropwise added into a solution of *p*-nitrophenyl chloroformate-functionalized PEG (2.0 g, 1.0 mmol) in DMSO (5 mL) which was obtained by treating PEG with *p*-nitrophenyl chloroformate in dichloromethane at 25 °C. After the mixture stirring at 25 °C for 48 h, the extensive dialysis of PEG-SS-NH_2 solution against water (MWCO 1000) was carried out and PEG-SS-NH_2 was obtained by freeze drying process. Yield: 85.4%. M_n (GPC) = 2.1 kDa, M_n (^{1}H-NMR) = 2.18 kDa, M_w/M_n(GPC) = 1.11. FT-IR (KBr): ν(cm^{-1}) 2872 and 1469 (methylene -C-H), and 1110 (ether bond C-O-C). ^{1}H-NMR ($CDCl_3$): δ 4.23 (-CH_2-O-C(O)-), 3.64 (-CH_2CH_2O-), 3.56 (-CH_2-NH-C(O)-), 3.38 (-OCH_3), 3.19 (-CH_2NH_2), 2.95 (-CH_2-SS-CH_2-).

Scheme 2. Synthesis of the PTTMA-*g*-SS-PEG Graft Copolymer by (I) RAFT Copolymerization and (II) Coupling Reaction[a]

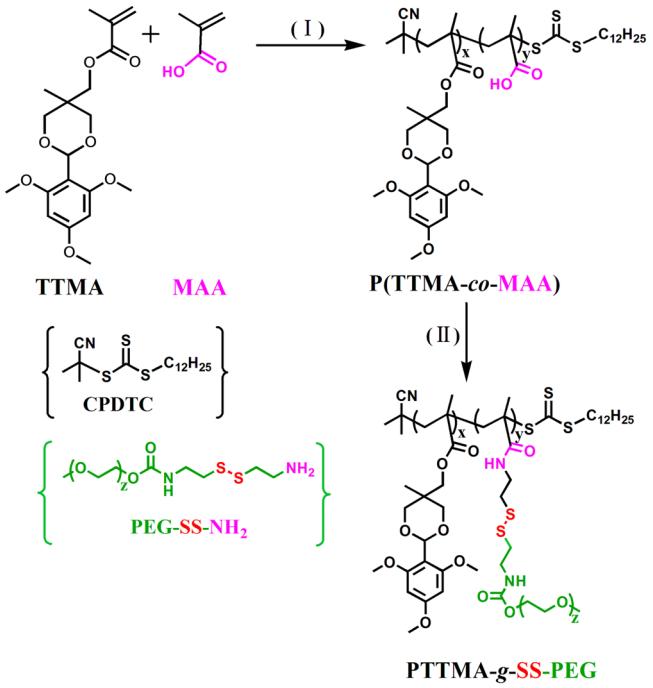

[a]Reagents and conditions: (I) RAFT copolymerization: toluene, n(CPDTC)/n(AIBN) = 5/1, 65 °C, 24 h; (II) coupling reaction: PEG-SS-NH_2, DMSO, n(EDC)/n(NHS) = 3/1, 25 °C, 48 h.

Synthesis of PTTMA-g-SS-PEG. Amphiphilic PTTMA-*g*-SS-PEG graft copolymer was prepared via high yielding amide coupling reaction of PEG-SS-NH_2 with P(TTMA-*co*-MAA) using EDC and NHS as a catalytic system. Briefly, P(TTMA-*co*-MAA) (0.5 g, 50 μmol), NHS (40.0 mg, 0.35 mmol), EDC (201.6 mg, 1.05 mmol), and PEG-SS-NH_2 (1.6 g, 0.8 mmol) were mixed in DMSO (10 mL) under a N_2 atmosphere at 25 °C for 48 h. The PTTMA-*g*-SS-PEG graft copolymer was isolated via dialysis technique (MWCO 3500) to remove excess PEG-SS-NH_2. Finally, PTTMA-*g*-SS-PEG graft copolymer was obtained after lyophilization. Yield: 93.0%. M_n (GPC) = 24.8 kDa, M_n (^{1}H-NMR) = 24.1 kDa, M_w/M_n(GPC) = 1.36. FT-IR (KBr): ν(cm^{-1}) 2945, 738, and 666 (aromatic -C-H), 2872 and 1469 (methylene -C-H of PEG), 2840 and 1367 (methylic −C-H), 1726 (carbonyl -C═O), 1609 (aromatic -C-C-), 1110 (ether bond C-O-C), and 1030 (-O-CH_3). ^{1}H-NMR ($CDCl_3$): 6.06 (aromatic protons), 5.89 (Ar-CH-), 3.76 (Ar-OCH_3), 3.64 (PEG), 3.38 (PEG, -OCH_3), 1.85 ((CH_3)$_2$C-, -CH_2CCH_2-), 1.22 (-$(CH_2)_{10}$-). PTTMA-*g*-PEG graft copolymer was prepared as a reduction-unresponsive control by the coupling reaction of P(TTMA-*co*-MAA) with PEG-OH in DMSO at 25 °C under the catalytic condition of DCC and DMAP.

Characterization. Fourier transform infrared spectra (FT-IR) were recorded using KBr disks in the region of 4000−500 cm^{-1} on BIO-RAD FT-IR 3000 spectrometer (BIO-RAD Company, Hercules, USA). ^{1}H-NMR spectra of the copolymers were measured on a Varian INOVA 500 MHz spectrometer (Varian Inc., Palo Alto, USA) using deuterated chloroform ($CDCl_3$) as solvents and tetramethylsilane (TMS) as the internal standard. The molecular weight (M_w, M_n) and molecular weight polydispersity index (M_w/M_n) of the products were measured by a Waters 1515 gel permeation chromatographer (GPC, Waters company, Milford, USA) equipped with refractive index detector, using PLgel MIXED C (MW 200-3M), PLgel C (MW500-20K) and PLgel C (MW4-400K) column. The measurements were

performed using a series of narrow polystyrene standards for the calibration of the columns and THF as the eluent at a flow rate of 1.0 mL/min at 25 °C. The size and size distribution of NPs were conducted by dynamic laser scattering (DLS) on a Brookhaven BI-200SM (Brookhaven Instruments Co., Holtsville, USA) at λ = 532 nm with a fixed detector angle of 90°. The morphology of NPs was investigated by transmission electron microscopy (TEM) on a JEOL JEM-1011 transmission electron microscope with an accelerating voltage of 100 kV. A drop of the NPs solution (1.0 mg/mL) was deposited onto a 400 mesh copper grid coated with carbon and allowed to dry in air at 25 °C before measurements.

Formation and Characterization of NPs. PTTMA-*g*-SS-PEG NPs were prepared by a nanoprecipitation method. Briefly, amphiphilic copolymer (10.0 mg) was dissolved in 1.0 mL of THF and dropwise added into 10 mL of 10 mM phosphate buffer (PB, pH 7.4) under stirring at 25 °C. The mixture solution was further stirred overnight to allow complete evaporation of organic solvents.

Critical micelle concentration (CMC) was investigated by steady-state fluorescent-probe methodology using pyrene as a probe on a Varian fluorescence spectrophotometer at room temperature.[34,35] PTTMA-*g*-SS-PEG graft copolymer concentrations for fluorescence investigation were varied from 2.0×10^{-5} to 0.2 mg/mL and the final pyrene concentration of 6.0×10^{-7} mmol/mL was fixed. These solutions were shaken vigorously and then allowed to equilibrate at 25 °C for at least 24 h. The pyrene excitation spectra with different copolymer concentrations were measured at the detection emission wavelength (λ_{em}= 373 nm). The CMC value was evaluated from the intersection of the tangent to the horizontal line of I_{337}/I_{331} with relative constant value and the diagonal line with rapidly increased I_{337}/I_{331} ratio.

pH-Triggered Hydrolysis of CBAs in the NPs. The CBAs hydrolysis, according to the previous report,[27] was followed by UV/vis spectroscopy by measuring the absorbance at 292 nm. The PTTMA-*g*-SS-PEG NPs solutions (1.0 mg/mL) were prepared and equally divided into three groups (2.0 mL). The solution with pH 5.0 was adjusted by addition of appropriate acetate buffer (4.0 M, pH 5.0) or maintained at pH 7.4 using phosphate buffer without/with 10 mM DTT, respectively. The samples were treated at 37 °C with shaking at 250 rpm. 80 μL aliquot was taken out at desired intervals of time and diluted with 3.5 mL 10 mM PB solution (pH 7.4). The absorbance at 292 nm was monitored. At the end, all the samples after addition of two drops of concentrated HCl were considered as complete hydrolysis of CBAs hydrolysis and the absorbance was measured to calculate the degree of acetal hydrolysis.

Reduction-Induced Detachment of PEG from PTTMA-*g*-SS-PEG NPs. The shedding of PEG from PTTMA-*g*-SS-PEG NPs via breakage of the disulfide linkage was examined by GPC, according to our previous report.[33] Under a N_2 atmosphere, PTTMA-*g*-SS-PEG NPs prepared as described above was incubated in 10 mM PB (pH 7.4) with 10 mM DTT. After 24 h, the residue in NPs suspension was collected by filtration. The resulting polymer after freeze-drying was characterized by GPC.

pH and Redox-Triggered Changes in Size of PTTMA-*g*-SS-PEG NPs. The changes in size of PTTMA-*g*-SS-PEG NPs induced by redox and/or pH were measured by DLS measurements. The NPs solutions at pH 7.4 and 5.0 without/with 10 mM DTT were prepared as above. The samples were gently stirred. The time-dependence size changes of NPs were obtained by DLS.

Loading and Release of CUR. CUR was used as a model hydrophobic anticancer agent for drug loading. CUR-loaded amphiphilic copolymer NPs were also prepared by a nanoprecipitation technique. Typically, amphiphilic copolymer (20.0 mg) and CUR (4.0 mg) were dissolved in 2.0 mL of THF and dropwise added into 20 mL of 10 mM PB solution (pH 7.4) under stirring at 25 °C. The solution was stirred overnight and then vacuumed for 1 h to allow completely evaporate THF. Then, the solution was filtered and lyophilized. For determination of drug loading content (DLC) and drug loading encapsulation efficiency (DLE), the lyophilized powder of NPs was dissolved in THF and analyzed with a UV/vis spectrophotometer at 425 nm using a standard curve method.[36] The DLC and DLE of the drug loaded NPs were calculated according to eqs 1 and 2, respectively

$$\mathrm{DLC}(\%) = (\text{amount of loaded drug}) / (\text{amount of drug-loaded NPs}) \times 100\% \quad (1)$$

$$\mathrm{DLE}(\%) = (\text{amount of loaded drug}) / (\text{total amount of feeding drug}) \times 100\% \quad (2)$$

The in vitro release of CUR from PTTMA-*g*-SS-PEG NPs was evaluated under five different conditions at 37 °C, i.e., (i) PB buffer (pH 7.4, 10 mM), (ii) acetate buffer (pH 5.0, 10 mM), (iii) PB buffer (pH 7.4, 10 mM) with 20 μM DTT, (iv) PB buffer (pH 7.4, 10 mM) with 10 mM DTT, and (v) acetate buffer (pH 5.0, 10 mM) with 10 mM DTT. CUR-loaded NPs suspension was divided into three aliquots and immediately transferred to a dialysis tube with a MWCO 8 000−14 000 Da. The dialysis tube was immersed into 20 ml of PB buffer (pH 7.4,10 mM) containing Tween-80 (0.5% w/w) and shaken at 37 °C. Five milliliters of the release medium was taken out at desired intervals of time and replenished with an equal volume of fresh medium. The release media were perfused with nitrogen gas in order to avoid oxidation of DTT. The amount of released drug in the incubation medium was quantified by UV/vis spectrophotometer. The release experiments were conducted in triplicate.

Cell Uptake Studies. The cell uptakes of CUR-loaded PTTMA-*g*-SS-PEG NPs, CUR-loaded PTTMA-*g*-PEG NPs, and free CUR toward esophageal carcinoma (EC-109) cells were evaluated by confocal laser scanning microscopy (CLSM) and flow cytometric analyses.

For qualitative cellular uptake evaluations observed by CLSM, EC-109 cells were placed into 24-well plates (1×10^4 cells/well) and cultured for attachment under a humidified atmosphere of 5% CO_2 and 95% air for 24 h at 37 °C. The cells were treated with an equivalent CUR concentration (10 μg/mL) of free CUR and nanoparticulate CUR for 2, 4, and 8 h. Then 1.0 mL of PB (pH 7.4,10 mM) was used to rinse the cell monolayers for removing excess NPs or free CUR. This process was repeated three times. The observation analysis was carried out on a CLSM (Leica AF 6500, Leica Microsystems GmbH, Germany).

For flow cytometric analyses, EC-109 cells were placed into 24-well plates (2×10^5 cells/well) and cultured in 2.0 mL of complete Dulbecco's Modified Eagle's Medium (DMEM) under a humidified atmosphere of 5% CO_2 and 95% air for 24 h at 37 °C. The medium was then withdrawn and culture media with free CUR and CUR-loaded NPs were changed at equivalent CUR concentration of 10.0 μg/mL. The cells were incubated for additional 2, 4, and 8 h, followed by washing with 10 mM PB (pH 7.4) three times and harvested. The analysis was examined by flow cytometer on an FACS calibur (BD Biosciences US).

MTT Assays. The cytotoxicities of blank PTTMA-*g*-SS-PEG NPs toward EC-109 cells and human hepatoma (HepG-2) cells were measured by MTT assays. In brief, the cells were seeded into 96-well plates (7×10^3 cells/well) and incubated in 100.0 μL of complete DMEM under a humidified atmosphere of 5% CO_2 and 95% air for 24 h at 37 °C. The medium was then removed and culture media with different concentration (0−1.0 mg/mL) NPs solutions were changed. The cells were incubated for additional 48 h, followed by washing with PB (pH 7.4, 10 mM) three times and harvested. The absorbances of the solutions were obtained on a Bio-Rad 680 microplate reader at 570 nm. The cytotoxicities of the CUR-loaded PTTMA-*g*-SS-PEG NPs, CUR-loaded PTTMA-*g*-PEG NPs and free CUR against EC-109 and HepG-2 cells were also examined by MTT assays. The cells were seeded into 96-well plates (1×10^4 cells/well) and incubated in 200.0 μL of complete DMEM for 24 h. After the cells were washed with PB (pH 7.4, 10 mM), free CUR and nanoparticulate CUR were added at different CUR concentrations (0−100.0 μg/mL). Then all the treatment processes were identical to the previous procedure as mentioned above.

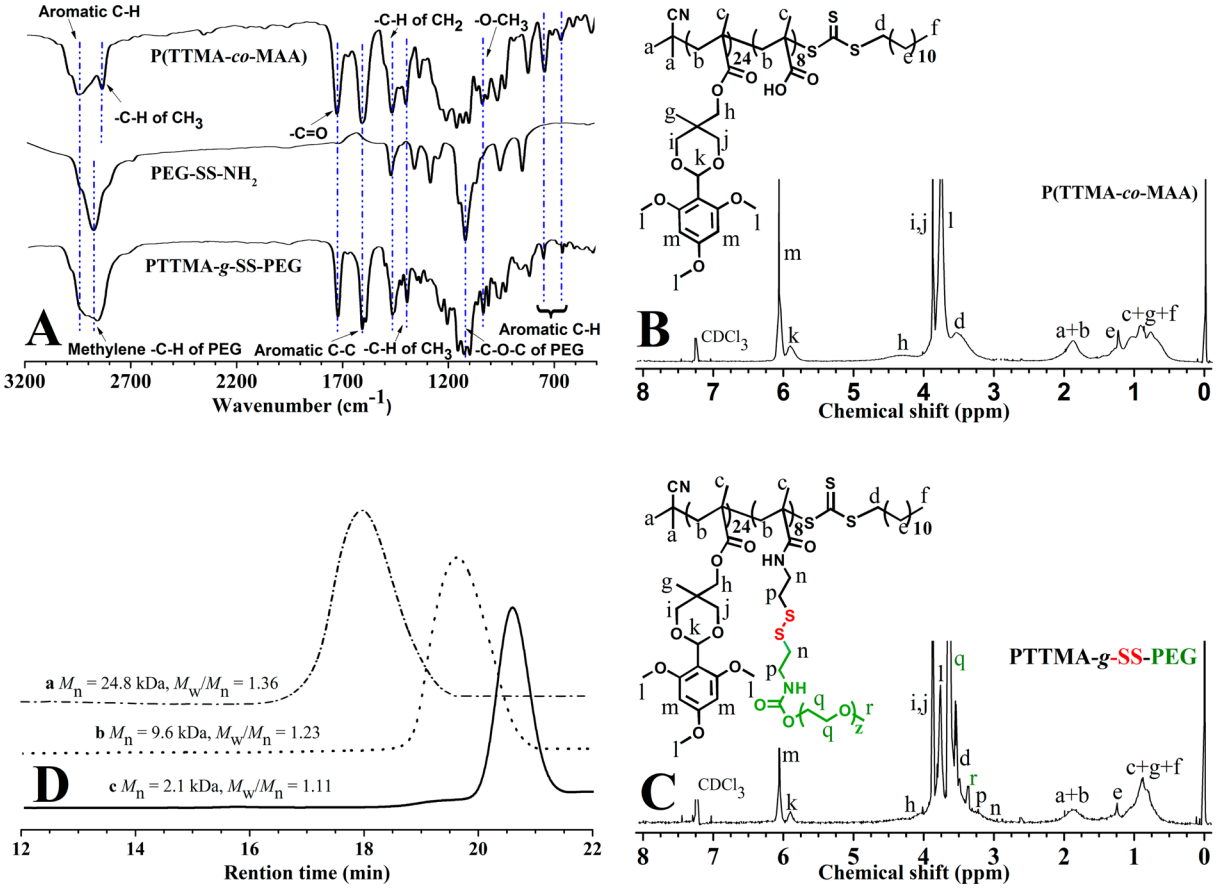

Figure 1. Chemical structure measurements. (A) FT-IR spectra, (B, C) ^{1}H-NMR spectra, and (D) GPC elution chromatograms of (a) PTTMA-*g*-SS-PEG, (b) P(TTMA-*co*-MAA), and (c) PEG-SS-NH$_2$, respectively.

Table 1. Characterization of PTTMA-*g*-SS-PEG and Reduction-Unresponsive PTTMA-*g*-PEG

entry	M_n (theory, kDa)	M_n (^{1}H-NMR^b, kDa)	M_n (GPC^c, kDa)	M_w/M_n (GPC^c)	size (nm)^d	PDI^d	CMC (μg/mL)^e
P(TTMA-*co*-MAA)^a	10.0	9.85	9.6	1.23			
PTTMA-*g*-SS-PEG	25.8	24.1	24.8	1.36	130.2	0.12	0.14
PTTMA-*g*-PEG	25.8	24.7	24.5	1.42	132.8	0.15	0.13

^{a}RAFT polymerization conditions: [TTMA]/[MAA]/[CPADN]/[AIBN] = 24.7/8.0/1.0/0.2 (mol/mol), toluene, 65 °C, 24 h. ^{b}Calculated from ^{1}H-NMR analysis. ^{c}Measured by GPC. ^{d}Determined by DLS. ^{e}Obtained by fluorescence microscopy using pyrene as a probe.

RESULTS AND DISCUSSION

Synthesis and Characterization of PTTMA-*g*-SS-PEG. In this study, we aimed to introduce a novel approach toward pH and reduction dual-induced disassemblable nanocarrier, which meanwhile combined the advantages of amphiphilic graft copoymer self-assembly NPs. As shown in Scheme 2, CBA-based moieties were introduced to the core forming backbone via RAFT copolymerization and PEG were coupled on the side chains by disulfide bonds, by which PTTMA-*g*-SS-PEG graft copolymer could be readily prepared. First, a carboxy-containing P(TTMA-*co*-MAA) was facilely synthesized through RAFT copolymerization of TTMA and MAA using CPDTC as a RAFT agent because of its well-controlled ability for the RAFT polymerizations of methacrylate derivatives.[32] Second, PTTMA-*g*-SS-PEG was obtained with a high yield through coupling reaction of PEG-SS-NH$_2$ and P(TTMA-*co*-MAA).

The chemical structure and composition of PTTMA-*g*-SS-PEG graft copolymer measured by FT-IR, ^{1}H-NMR, and GPC were shown in Figure 1, respectively. All typical peaks of both the PTTMA and PEG were visible in the FT-IR spectrum after coupling reaction of PEG-SS-NH$_2$ (Figure. 1A). The peak at 2945, 1609, and 738 cm^{-1} (aromatic -C-H and -C-C- stretching vibrations), 1367 cm^{-1} (asymmetric deformation vibrations of -C-H of CH$_3$), and 1030 cm^{-1} (stretching vibrations of -O-CH$_3$) demonstrated the existence of the PTTMA backbone. In comparison with the FT-IR spectrum before coupling reaction of PEG-SS-NH$_2$ as shown in Figure 1A, new peaks corresponding to PEG side chains were observed, among which the strongest peak at 1110 cm^{-1} belonged to the characteristic stretching vibration absorption of ether bond (C-O-C). Figure 1B showed the ^{1}H-NMR spectrum of the P(TTMA-*co*-MAA). The characteristic peaks of the PTTMA appeared at 6.05 ppm (m), 5.89 ppm (k), and 3.75 ppm (l), and a series of new resonance signals attributed to the protons of PEG side chains were found to be at 3.35 ppm (terminal OCH$_3$, r), 3.64 ppm (OCH$_2$CH$_2$O, q). The monomer conversion and number molecular weight (M_n) values of P(TTMA-*co*-MAA) and PTTMA-*g*-SS-PEG copolymers could be calculated by comparing the integrals for the peak of the hydrogen protons on the phenyl ring of TTMA (at about δ

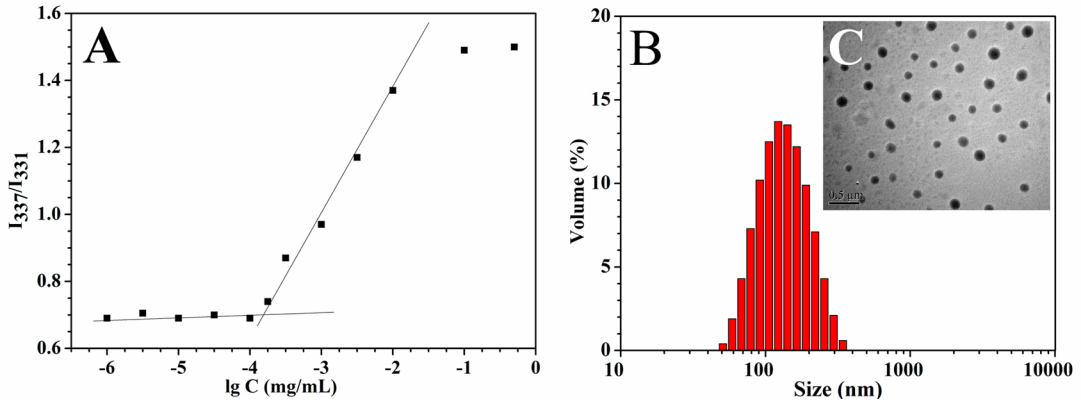

Figure 2. (A) Self-assembly of PTTMA-*g*-SS-PEG. The fluorescence intensity ratio I_{337}/I_{331} of pyrene versus the concentrations of copolymers in 10 mM phosphate buffer (pH 7.4) was used to evaluate CMC. Size distribution of NPs (1.0 mg/mL) and their morphology were measured by (B) DLS and (C) TEM, respectively.

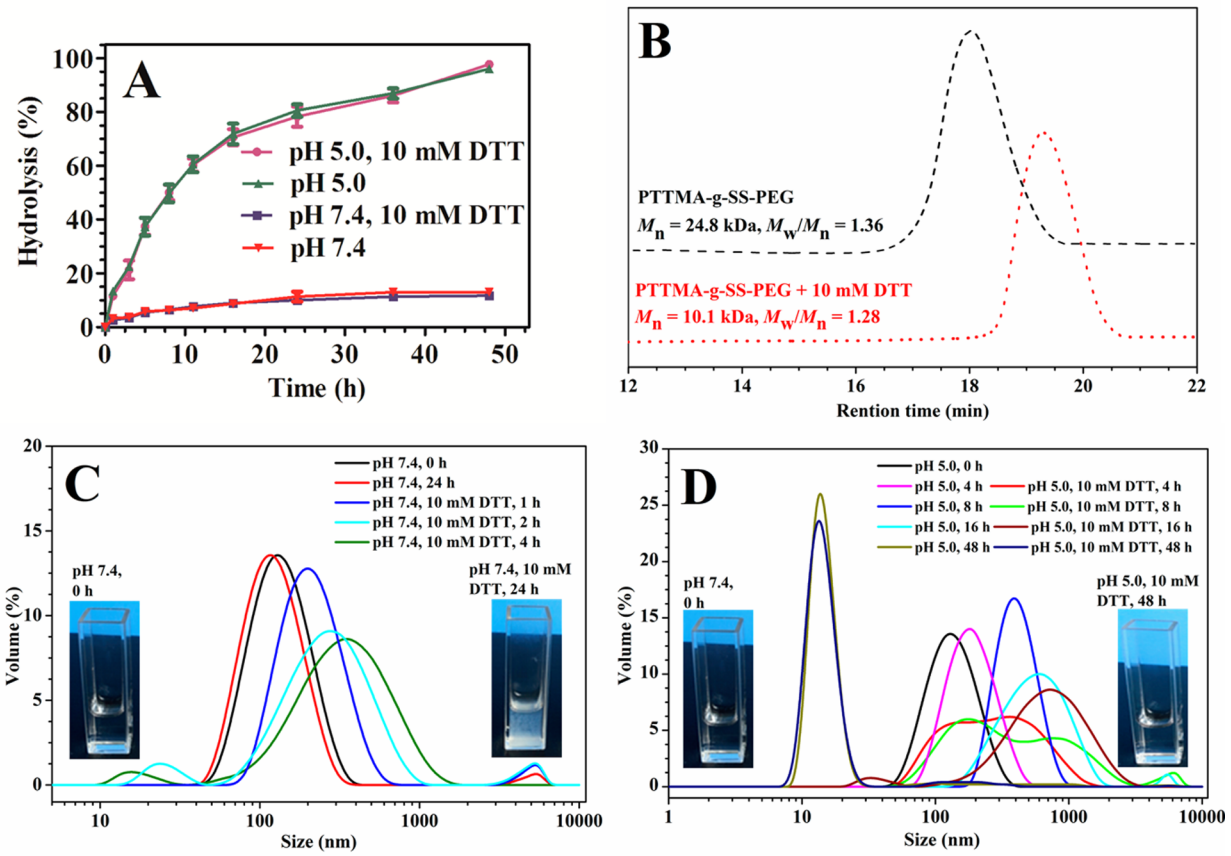

Figure 3. pH and reduction dual-induced disassembly of PTTMA-*g*-SS-PEG NPs. pH-Dependent CBAs hydrolysis measured by (A) UV/vis spectroscopy, (B) reduction-induced disassembly determined by GPC, and (C, D) size changes of NPs examined by DLS, respectively.

6.05, m), terminal methoxy protons of PEG (at about 3.35 ppm, r) with methylene protons of the CPDTC (at about δ = 1.22, e). As shown in Table 1, the molecular weight of PTTMA-*g*-SS-PEG was much higher than that of P(TTMA-*co*-MAA), indicating the successful proceeding of coupling reaction of PEG-SS-NH_2. Moreover, it was seen that all GPC curves were symmetrical and unimodal (Figure 1D) and their molecular weight distributions were narrow (M_w/M_n = 1.21−1.36), which meant the well-controlled nature of these RAFT and coupling reaction. Additionally, the M_n calculated from ^{1}H-NMR and the M_n determined by GPC were both well in agreement with the theoretical values (Table 1). Thus, the aforementioned results supported that PTTMA-*g*-SS-PEG graft copolymer possessed well-defined structure and controlled molecular weight via a combination of RAFT and coupling reaction.

PTTMA-*g*-PEG graft copolymer as a reduction-unresponsive control had a low M_w/M_n of 1.42 and a M_n of 24.5 kDa, close to that of PTTMA-*g*-SS-PEG (Table 1).

Self-Assembly Behavior of PTTMA-*g*-SS-PEG. Amphiphilic graft copolymers were a kind of interesting materials that could be self-assembled into various nano aggregates like

vesicles, spherical, and spindlelike micelles in aqueous solutions. The self-assembled behaviors could be controlled by changing the grafting densities and length of side chains.[37] The obtained PTTMA-*g*-SS-PEG graft copolymers could self-assemble into nano-sized NPs with hydrophobic PTTMA core and hydrophilic PEG shell by nanoprecipitation method. The NPs formation was first evaluated using pyrene as a fluorescent probe at pH 7.4. It has been reported that high sensitivity of a vibrational band contained in fluorescence spectra of pyrene solutions was dependent on the environmental polarity of the pyrene. The fluorescence intensity ratio I_{337}/I_{331} of pyrene versus the logarithmic concentrations of copolymers was used to estimate the CMC of PTTMA-*g*-SS-PEG graft copolymer, as shown in Figure 2A. No significant changes of I_{337}/I_{331} were observed in low PTTMA-*g*-SS-PEG concentration ranges. As the concentration increasing, the intensity ratios (I_{337}/I_{331}) of the pyrene excitation spectra increased markedly, indicating pyrene aggregation into the PTTMA core. The CMC values of PTTMA-*g*-SS-PEG and PTTMA-*g*-PEG were 0.14 and 0.13 μg/mL (Table 1), respectively. The low CMC value meant the NPs assembled from PTTMA-*g*-SS-PEG graft copolymer could retain the stability in very dilute bloodstream milieu, which was one of the significant features for in vivo drug delivery.[22,38]

The size distribution and morphology of the PTTMA-*g*-SS-PEG NPs were studied by DLS and TEM, respectively. DLS measurement (Figure 2B) showed that the average diameter of PTTMA-*g*-SS-PEG NPs was about 130.2 nm and their size distribution was narrow (PDI = 0.12) in 10 mM PB (pH 7.4). The size and size distribution of PTTMA-*g*-PEG NPs was similar with that of PTTMA-*g*-SS-PEG NPs (Table 1), due to their analogue chemical structures. The TEM image (Figure 2C) demonstrated that the PTTMA-*g*-SS-PEG NPs had a regular spherical shape and dispersed very well. The mean diameter was around 90 nm, which was smaller than that from DLS observations. This difference may be ascribed to the shrinkage of the PEG shell during sample preparation for TEM.[21]

pH and Reduction Dual-Induced Disassembly of PTTMA-*g*-SS-PEG NPs. Two unique features of PTTMA-*g*-SS-PEG copolymer were the acid-labile property due to the hydrolysis of CBAs and reduction-induced shedding of PEG via cleavage of disulfide bonds. The pH-dependent CBAs hydrolysis behaviors of PTTMA-*g*-SS-PEG NPs were studied by UV/vis spectroscopy measurements in pH 7.4 or pH 5.0 buffer solutions at 37 °C with the absence or presence of 10 mM DTT. It can be seen from Figure 3A that the CBAs hydrolysis rates of PTTMA-*g*-SS-PEG NPs were highly pH-dependent. Under physiological conditions (pH 7.4), the PTTMA-*g*-SS-PEG NPs was relatively stable and the CBAs hydrolysis rate was extremely low (12.8% in 48 h). In contrast, PTTMA-*g*-SS-PEG NPs in mildly acidic environments (pH 5.0) showed rapid CBAs hydrolysis with half-live of approximately 8.3 h at pH 5.0. Meanwhile, as shown in Figure 3A, the effects of 10 mM DTT contained in pH 7.4 and pH 5.0 buffer solutions on the CBAs hydrolysis behaviors of PTTMA-*g*-SS-PEG NPs were small or nonexistent, indicating that PEG shell or its shedding via cleavage of the disulfide bonds did not affect CBAs hydrolysis.[17]

The reduction-induced breaking of disulfide bonds existed in PTTMA-*g*-SS-PEG NPs was confirmed by GPC using PTTMA-*g*-SS-PEG NPs before the treatment and after by 10 mM DTT. The smaller molecular weight of the DTT treated PTTMA-*g*-SS-PEG was found in Figure 3B than that of the untreated one. This difference may be due to the fact that the successful cleavage of disulfide bonds resulted in detaching of PEG.[33]

Under mildly acidic and reductive conditions, pH and reduction dual-induced changes in chemical structure of PTTMA-*g*-SS-PEG would be advantageous to NPs complete disassembly. To investigate the synergistic effect, we traced the size changes of PTTMA-*g*-SS-PEG NPs in response to acidic pH and/or 10 mM DTT by DLS measurements. As shown in Figure 3C, under physiological conditions (pH 7.4) without 10 mM DTT, little size changes of PTTMA-*g*-SS-PEG NPs were observed over 24 h, which could be ascribed to the relatively stability of CBAs groups in alkaline media. However, under the same conditions with 10 mM DTT, the increase in size of PTTMA-*g*-SS-PEG NPs from 130 nm to about 202 nm in 2 h was found and the size reached about 362 nm in 4 h. The fast aggregation behaviors were ascribed to reduction-induced shedding of the PEG shell, resulting in rearrangement of the hydrophobic fragments (PTTMA) into larger aggregates.[39] Until 24 h, a significant portion of aggregates appeared, further indicating the disintegration of the NPs and the formation of large aggregates by hydrophobic interactions between PTTMA segments detached from the graft copolymer.

When PTTMA-*g*-SS-PEG NPs were treated in pH 5.0 with the absence of 10 mM DTT, significant changes of NPs sizes were observed in Figure 3D, wherein NPs swelled from 130 nm to about 176 nm in 4 h, and reached about 601 nm in 16 h. The swelling process was attributed to CBAs partial hydrolysis and thereafter the increase in hydrophilicity of PTTMA core. It should be noted that abundant small-sized particles (about 14 nm) were detected after incubation for 48 h, indicating that PTTMA-*g*-SS-PEG NPs were degraded into water-soluble unimers because of the complete CBAs hydrolysis.

Under mildly acidic (pH 5.0) and reductive (10 mM DTT) conditions, the fastest changes in size of PTTMA-*g*-SS-PEG NPs were also observed in Figure 3D. The increase in diameter of NPs from about 130 nm to about 370 nm after 4 h were seen and a large number of nano-aggregates with a size greater than 900 nm were found in 16 h. During this process, no precipitation was observed, which may be ascribed to the improved hydrophilicity of PTTMA core following CBAs hydrolysis. However, when the NPs suspension was incubated for 48 h, a large number of 13.0 nm particles were detected, indicating that PTTMA-*g*-SS-PEG NPs were inclined to form hydrophilic unimers after PEG shedding and complete CBAs hydrolysis.[26]

Drug Loading and pH/Reduction Dual-Triggered Drug Release. CUR, as a model natural chemotherapeutic agent, was used to evaluate the loading and releasing properties of PTTMA-*g*-SS-PEG NPs as a dual stimuli-responsive nanocarrier. As mentioned above for CUR, a prominent anticancer candidate, improving its solubility in water, avoiding its degradation at physiological pH before being delivered into the tumor cells and excellent loading efficiency are the important issues to be addressed for the nanocarrier systems.[40] In this study, PTTMA-*g*-SS-PEG graft copolymer NPs would be expected to be capable of effective loading and delivering CUR. The characteristics of the CUR-loaded NPs, including loading content, encapsulation efficiency, the mean diameter and size distribution were summarized in Table 2. Excitedly, the CUR loading capacity of PTTMA-*g*-SS-PEG NPs ranged from 4.8 to 19.2% with high encapsulation efficiencies ranged from 92.0 to 98.0%. The results also showed that the particle sizes of

Table 2. Characterization of CUR-Loaded PTTMA-*g*-SS-PEG and PTTMA-*g*-PEG NPs

entry	DLC (%) theory	DLC (%) determined[a]	DLE (%)[a]	size[b] (nm)	PDI[b]
PTTMA-*g*-SS-PEG	5	4.8	96.0	125.3 ± 2.3	0.14
	10	9.7	97.0	142.6 ± 4.1	0.16
	20	19.2	96.0	158.4 ± 5.1	0.27
PTTMA-*g*-PEG	5	4.6	92.0	129.4 ± 3.2	0.13
	10	9.8	98.0	152.3 ± 4.6	0.21
	20	19.4	97.0	161.5 ± 5.7	0.28

[a]DLC and DLE of CUR measured by UV/vis spectrophotometer. [b]The size and PDI of the NPs were obtained by DLS.

CUR-loaded PTTMA-*g*-SS-PEG NPs showed slight increase from 125 to 158 nm when the CUR loading amount increased from 4.8 to 19.2%. And all the PDI remained in a narrow range of 0.14−0.28. The similar CUR loading efficiencies were also observed for PTTMA-*g*-PEG NPs. The excellent encapsulation efficiency and high drug loading capacity for PTTMA-*g*-SS-PEG NPs and PTTMA-*g*-PEG NPs might be due to the strong $\pi-\pi$ conjugate action between CUR and the phenyl ring in the PTTMA.[41] Additionally, all drug-loaded NPs were no more than 200 nm, which were conducive to increase passive tumor targeting via enhanced permeation and retention (EPR) effect.[42]

The in vitro CUR release profiles from drug-loaded PTTMA-*g*-SS-PEG NPs were investigated by the dialysis method at pH 7.4 and 5.0 media without or with DTT, as shown in Figure 4.

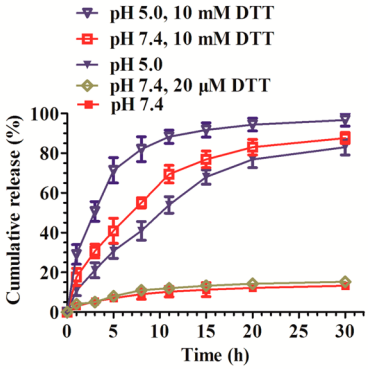

Figure 4. Redox and/or pH-triggered in vitro CUR release from PTTMA-*g*-SS-PEG NPs in response to different DTT concentrations and pH at DLC of 4.8%.

In the presence or absence of 20 μM DTT, the cumulative release of CUR at pH 7.4 was less than of 15% within 20 h, and there was no further release tendency until 30 h. The slow release indicated that the CUR-loaded PTTMA-*g*-SS-PEG NPs would preserve their stable nanostructure at physiological pH (7.4, mimicking the blood circulation), which could result in reduced drug loss in extracellular environments. However, 76.8% of CUR was released in 20 h at pH 5.0 (mimicking the acidic intracellular endosome/lysosome compartments),[43] and 83.1% of CUR was also boosted released under a reducing environment (10 mM DTT and pH 7.4, mimicking the reductive environment of cytoplasm) in 20 h. Interestingly, under mildly acidic (pH 5.0) and reductive (10 mM DTT) conditions (mimicking the intracellular microenvironment), the release of CUR was further improved to 94.3 % in 20 h, which might be due to synergistic effect of pH and reduction dual-induced disassembly of NPs.

Therefore, PTTMA-*g*-SS-PEG NPs could provide efficient protection for the loaded CUR, and fast release CUR in an intracellular dual-triggered condition (10.0 mM DTT and pH 5.0), indicating the combination use of redox and pH responsiveness was very beneficial for the enhanced and controlled intracellular drug release in tumor cells.

This pH and reduction dual-triggered drug release behavior for achieving success in the intracellular drug delivery with nanotechnology is particularly interesting. Almost all of the drugs loaded in NPs are expected to remain in the internal of NPs when the intravenously administered NPs circulated at physiological pH, thus prolonging circulation time of drugs in vivo and beneficial for minimizing drug loss in circulation. Once the NPs reach the tumor site and are internalized inside the cells, fast drug release is desired through NPs disassembly stimulated by the mildly acidic environment and the high reducing agent GSH concentration inside tumor cell, which may improve the therapeutic efficacy in vivo. Therefore, with the sensitive pH and reduction dual-induced disassemblable properties, PTTMA-*g*-SS-PEG NPs may provide a promising targeted and controlled delivery approach for many anticancer therapeutics.

Intracellular CUR Release. To evaluate the cellular internalization and the dual-triggered intracellular release of CUR, we incubated the CUR-loaded PTTMA-*g*-SS-PEG NPs with EC-109 cells using CLSM, as showed in Figure 5. The cells treated by CUR-loaded PTTMA-*g*-PEG NPs and free CUR were used as controls. As expected, the strongest intracellular CUR fluorescence appeared in the cytoplasm and in the nucleus was found in EC-109 cells incubated for 2 h with the CUR-loaded PTTMA-*g*-SS-PEG NPs. In contrast, secon-

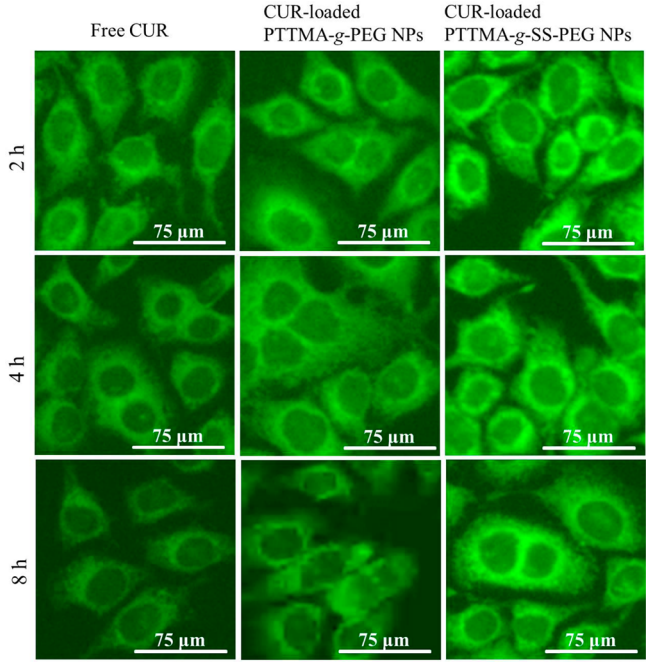

Figure 5. Representative images under fluorescence microscope of EC-109 cells incubated with CUR-loaded PTTMA-*g*-SS-PEG NPs, CUR-loaded PTTMA-*g*-PEG NPs, and free CUR at equivalent CUR concentration of 10.0 μg/mL for 2, 4, or 8 h.

dary CUR fluorescence intensity was shown mainly in the cytoplasm of the cells incubated with the CUR-loaded PTTMA-*g*-PEG NPs and the weakest fluorescence was found in the cytoplasm of the cells treated by free CUR for 2 h. The time-dependent cellular uptake was examined after 4 or 8 h, and it was observed the fluorescence intensity in the cell treated with free CUR was gradually decreased with incubation time lasted, and sustaining fluorescence intensity with time was viewed in the cells treated by CUR-loaded PTTMA-*g*-PEG and PTTMA-*g*-SS-PEG NPs. Besides the superiority of nano-sized particles readily internalized in cells by an endocytosis pathway mechanism,[44] the strongest intracellular fluorescence for the cells incubated with CUR-loaded PTTMA-*g*-SS-PEG NPs might be ascribed to the quick and larger amount of intracellular released CUR, which was dual-triggered by pH and reduction. Furthermore, the stronger intracellular fluorescence also indicated that CUR encapsulated in NPs, especially for PTTMA-*g*-SS-PEG, exhibited excellent bioavailability than free CUR. These results can be also confirmed by flow cytometric analyses (Figure 6) of the cells incubated with free CUR, CUR-loaded PTTMA-*g*-PEG NPs, CUR-loaded PTTMA-*g*-SS-PEG NPs.

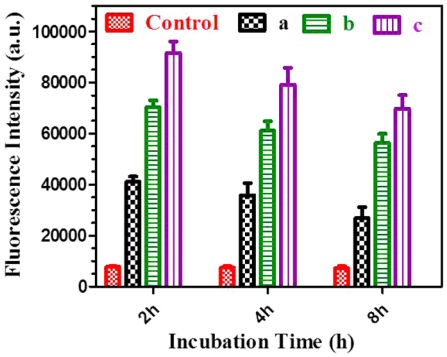

Figure 6. Comparative analysis of the mean fluorescence intensity on EC-109 cells after treatment with (a) free CUR, (b) CUR-loaded PTTMA-*g*-PEG NPs, and (c) CUR-loaded PTTMA-*g*-SS-PEG NPs at different incubation time measured by flow cytometry.

Cell Growth Inhibition Assay in Vitro. To evaluate the biocompatibility of the copolymer, the in vitro cytotoxicities of blank PTTMA-*g*-SS-PEG and PTTMA-*g*-PEG NPs toward EC-109 cells and HepG-2 cells were evaluated by MTT assays. Figure 7 showed the viability of cells incubated with NPs at various concentrations levels for 48 h. The results displayed that both of the blank NPs did not exhibit obvious inhibition effects (cell viabilities ≥95%) on cell proliferation at concentrations up to 1.0 mg/mL. With the good biocompatibility, PTTMA-*g*-SS-PEG NPs can be used as safe drug nanocarriers for cancer therapy.

The in vitro cellular proliferation inhibition of CUR-loaded PTTMA-*g*-SS-PEG NPs against EC-109 cells and HepG-2 cells was also estimated by MTT assays (Figure 8 and Table 3). In contrast to free CUR, CUR-loaded PTTMA-*g*-SS-PEG NPs exhibited higher inhibition efficiencies both for EC-109 cells and HepG-2 cells, whereas CUR-loaded PTTMA-*g*-PEG NPs showed slightly lower or higher inhibition efficiency than free CUR in EC-109 cells and HepG-2 cells, respectively. The results revealed that the faster CUR release from the CUR-loaded PTTMA-*g*-SS-PEG NPs triggered by endo/lysosomal pH and intracellular reducing environment enhanced the inhibition of the cellular proliferation. Additionally, it was worth mentioning that the research on nanoparticle-based CUR formulations for cellular proliferation inhibition of EC-109 cells was still rarely reported. The results here indicated that CUR-loaded NPs, especially for PTTMA-*g*-SS-PEG, had obvious inhibitory effect on EC-109 cells. With regard to inhibiting HepG-2 cells proliferation, the IC_{50} value (3.16 μg/mL) of CUR-loaded PTTMA-*g*-SS-PEG NPs was lower than those previous reported nanoparticulate CUR formulations (22.0 μg/mL[45] and 6.63 μg/mL[46]). Furthermore, the antitumor activity of nanoparticulate CUR can be further improved by introducing some targeting ligands (e.g., monoclonal antibodies, peptides, and folic acids) into the surface of CUR-loaded PTTMA-*g*-SS-PEG NPs to promote specific and efficient cellular uptake of NPs.

CONCLUSIONS

PTTMA-*g*-SS-PEG amphiphilic graft copolymer with CBAs-functionalized PTTMA backbone and disulfilde linkaged PEG side chains was successfully prepared by combining RAFT polymerization and coupling reaction, by which pH and reduction dual-induced disassemblable NPs were fabricated for tumor intracellular drug delivery. The obtained PTTMA-*g*-SS-PEG with low CMC were relatively stable under normal physiological conditions (pH 7.4), and rapidly swell and completely disassemble into water-soluble unimers via acetal hydrolysis at pH 5.0, which could be further enhanced by PEG detaching at presence of 10 mM DTT. PTTMA-*g*-SS-PEG NPs could effectively encapsulate anticancer drug of CUR with drug loading content up to 19.2% and high entrapment efficiency of

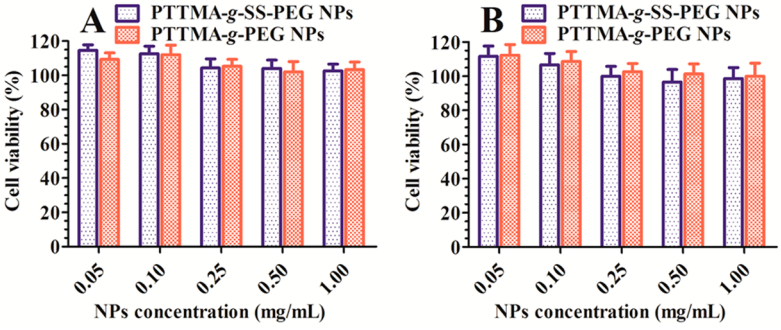

Figure 7. In vitro cytotoxicity of blank PTTMA-*g*-SS-PEG and PTTMA-*g*-PEG NPs toward (A) EC-109 cells and (B) HepG-2 cells. The cells were incubated with NPs for 48 h. Data are presented as the average ± standard deviation (n = 5).

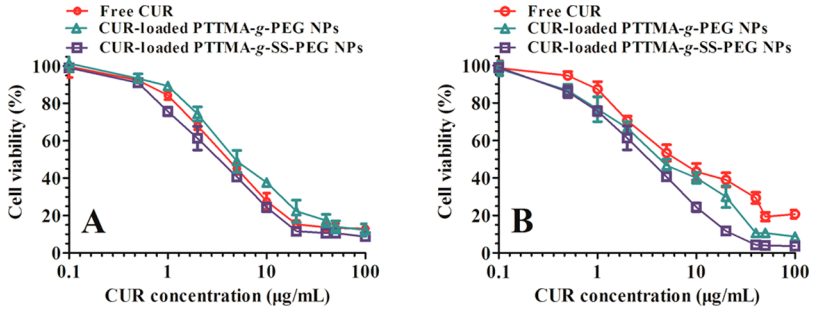

Figure 8. Cell growth inhibition activity of CUR-loaded PTTMA-*g*-SS-PEG NPs, CUR-loaded PTTMA-*g*-PEG NPs, and free CUR as a function of CUR dosages toward (A) EC-109 cells and (B) HepG-2 cells. The cells were incubated with CUR-loaded NPs or free CUR for 48 h. Data are presented as the average ± standard deviation (n = 5).

Table 3. IC_{50} Values of Nanoparticulate CUR and Free CUR toward EC-109 cells and HepG-2 cells as Measured by MTT Assays

	IC_{50} (μg/mL)	
entry	EC-109	HepG-2
free CUR	4.27	6.46
PTTMA-*g*-PEG	4.90	4.27
PTTMA-*g*-SS-PEG	3.31	3.16

92.0%, partly due to the strong $\pi-\pi$ conjugate action of CUR with phenyl in the hydrophobic PTTMA main chain. Under normal physiological conditions, CUR release was inhibited due to structural stability of CUR-loaded PTTMA-*g*-SS-PEG NPs, whereas under intracellular mildly acidic (pH 5.0) and reductive (10 mM DTT) environments, the CUR was released fast because of the dual-triggered NPs disassembly, leading to enhanced growth inhibition toward EC-109 cells and HepG-2 cells. Hence, these pH and reduction dual-induced disassemblable PTTMA-*g*-SS-PEG graft copolymer NPs possessed several favorable properties as a kind of ideal drug carriers, such as the controlled synthesis, low CMC, good biocompatibility, excellent drug loading efficiency, minimal drug leakage during circulation, enhanced drug release in response to the intracellular mildly acidic and reductive microenvironment, which are highly interesting as effective vehicles for activated intracellular drug release.

AUTHOR INFORMATION

Corresponding Author

*E-mail: ajdong@tju.edu.cn. Fax: +86 22 27890710. Tel: +86 22 27890706.

Author Contributions

†J.Z. and J.L. contributed equally to this work.

Notes

The authors declare no competing financial interest.

ACKNOWLEDGMENTS

This work was supported by the grants from the National Natural Science Foundation of China (51103097, 31271073, 81301309, 81371667) and Specialized Research Fund for the Doctoral Program of Higher Education of China (20120032110013).

REFERENCES

(1) Ge, Z.; Liu, S. *Chem. Soc. Rev.* **2013**, *42*, 7289−7325.
(2) Wang, W.; Cheng, D.; Gong, F.; Miao, X.; Shuai, X. *Adv. Mater.* **2012**, *24*, 115−120.
(3) Li, Y.; Gao, G. H.; Lee, D. S. *Adv. Healthcare Mater.* **2013**, *2*, 388−417.
(4) Yu, S.; He, C.; Ding, J.; Cheng, Y.; Song, W.; Zhuang, X.; Chen, X. *Soft Matter* **2013**, *9*, 2637−2645.
(5) Qiao, Z. Y.; Zhang, R.; Du, F. S.; Liang, D. H.; Li, Z. C. *J. Controlled Release* **2011**, *152*, 57−66.
(6) Cheng, R.; Meng, F.; Deng, C.; Klok, H. A.; Zhong, Z. *Biomaterials* **2013**, *34*, 3647−3657.
(7) Dai, J.; Lin, S.; Cheng, D.; Zou, S.; Shuai, X. *Angew. Chem., Int. Ed.* **2011**, *50*, 9404−9408.
(8) Binauld, S.; Stenzel, M. H. *Chem. Commun.* **2013**, *49*, 2082−2102.
(9) Lee, S. F.; Zhu, X. M.; Wang, Y. X. J.; Xuan, S. H.; You, Q.; Chan, W. H.; Wong, C. H.; Wang, F.; Yu, J. C.; Cheng, C. H. K.; Leung, K. C. F. *ACS Appl. Mater. Interfaces* **2013**, *5*, 1566−1574.
(10) Wei, H.; Zhuo, R. X.; Zhang, X. Z. *Prog. Polym. Sci.* **2013**, *38*, 503−535.
(11) Ding, J.; Chen, J.; Li, D.; Xiao, C.; Zhang, J.; He, C.; Zhuang, X.; Chen, X. *J. Mater. Chem. B* **2013**, *1*, 69−81.
(12) Li, J.; Huo, M.; Wang, J.; Zhou, J.; Mohammad, J. M.; Zhang, Y.; Zhu, Q.; Waddad, A. Y.; Zhang, Q. *Biomaterials* **2012**, *33*, 2310−2320.
(13) Yue, J.; Wang, R.; Liu, S.; Wu, S.; Xie, Z.; Huang, Y.; Jing, X. *Soft Matter* **2012**, *8*, 7426−7435.
(14) Pisoni, R. L.; Acker, T. L.; Lisowski, K. M.; Lemons, R. M.; Thoene, J. G. *J. Cell Biol.* **1990**, *110*, 327−335.
(15) Zhang, J.; Wu, L.; Meng, F.; Wang, Z.; Deng, C.; Liu, H.; Zhong, Z. *Langmuir* **2011**, *28*, 2056−2065.
(16) Pan, Y. J.; Chen, Y. Y.; Wang, D. R.; Wei, C.; Guo, J.; Lu, D. R.; Chu, C. C.; Wang, C. C. *Biomaterials* **2012**, *33*, 6570−6579.
(17) Chen, W.; Zhong, P.; Meng, F.; Cheng, R.; Deng, C.; Feijen, J.; Zhong, Z. *J. Controlled Release* **2013**, *169*, 171−179.
(18) Liang, K.; Such, G. K.; Zhu, Z.; Yan, Y.; Lomas, H.; Caruso, F. *Adv. Mater.* **2011**, *23*, H273−H277.
(19) Wu, Y.; Chen, W.; Meng, F.; Wang, Z.; Cheng, R.; Deng, C.; Liu, H.; Zhong, Z. *J. Controlled Release* **2012**, *164*, 338−345.
(20) Chen, W.; Zou, Y.; Jia, J.; Meng, F.; Cheng, R.; Deng, C.; Feijen, J.; Zhong, Z. *Macromolecules* **2013**, *46*, 699−707.
(21) Guo, S.; Qiao, Y.; Wang, W.; He, H.; Deng, L.; Xing, J.; Xu, J.; Liang, X. J.; Dong, A. *J. Mater. Chem.* **2010**, *20*, 6935−6941.
(22) Cheng, R.; Wang, X.; Chen, W.; Meng, F.; Deng, C.; Liu, H.; Zhong, Z. *J. Mater. Chem.* **2012**, *22*, 11730−11738.
(23) Gillies, E. R.; Jonsson, T. B.; Fréchet, J. M. J. *J. Am. Chem. Soc.* **2004**, *126*, 11936−11943.
(24) Gillies, E. R.; Frechet, J. M. J. *Chem. Commun.* **2003**, *14*, 1640−1641.
(25) Chen, W.; Meng, F.; Li, F.; Ji, S. J.; Zhong, Z. *Biomacromolecules* **2009**, *10*, 1727−1735.
(26) Du, Y.; Chen, W.; Zheng, M.; Meng, F.; Zhong, Z. *Biomaterials* **2012**, *33*, 7291−7299.
(27) Griset, A. P.; Walpole, J.; Liu, R.; Gaffey, A.; Colson, Y. L.; Grinstaff, M. W. *J. Am. Chem. Soc.* **2009**, *131*, 2469−2471.

(28) Yallapu, M. M.; Jaggi, M.; Chauhan, S. C. *Drug Discovery Today* **2012**, *17*, 71−80.
(29) Anand, P.; Sundaram, C.; Jhurani, S.; Kunnumakkara, A. B.; Aggarwal, B. B. *Cancer Lett.* **2008**, *267*, 133−164.
(30) Gou, M.; Men, K.; Shi, H.; Xiang, M.; Zhang, J.; Song, J.; Long, J.; Wan, Y.; Luo, F.; Zhao, X.; Qian, Z. *Nanoscale* **2011**, *3*, 1558−1567.
(31) Tang, H.; Murphy, C. J.; Zhang, B.; Shen, Y.; Van Kirk, E. A.; Murdoch, W. J.; Radosz, M. *Biomaterials* **2010**, *31*, 7139−7149.
(32) Chong, Y. K.; Moad, G.; Rizzardo, E.; Thang, S. H. *Macromolecules* **2007**, *40*, 4446−4455.
(33) Lin, D.; Jiang, Q.; Cheng, Q.; Huang, Y.; Huang, P.; Han, S.; Guo, S.; Liang, Z.; Dong, A. *Acta Biomater.* **2013**, *8*, 7746−7757.
(34) Chang, L.; Deng, L.; Wang, W.; Lv, Z.; Hu, F.; Dong, A.; Zhang, J. *Biomacromolecules* **2012**, *13*, 3301−3310.
(35) Chen, J.; Ouyang, J.; Kong, J.; Zhong, W.; Xing, M. M. *ACS Appl. Mater. Interfaces* **2013**, *5*, 3108−3117.
(36) Das, R. K.; Kasoju, N.; Bora, U. *Nanomed.: Nanotech. Biol. Med.* **2010**, *6*, 153−160.
(37) Feng, C.; Li, Y.; Yang, D.; Hu, J.; Zhang, X.; Huang, X. *Chem. Soc. Rev.* **2011**, *40*, 1282−1295.
(38) Yang, Y. Q.; Guo, X. D.; Lin, W. J.; Zhang, L. J.; Zhang, C. Y.; Qian, Y. *Soft Matter* **2012**, *8*, 454−464.
(39) Wen, H. Y.; Dong, H. Q.; Xie, W.; Li, Y. Y.; Wang, K.; Pauletti, G. M.; Shi, D. L. *Chem. Commun.* **2011**, *47*, 3550−3552.
(40) Mohanty, C.; Sahoo, S. K. *Biomaterials* **2010**, *31*, 6597−6611.
(41) Sun, Y.; Yan, X.; Yuan, T.; Liang, J.; Fan, Y.; Gu, Z.; Zhang, X. *Biomaterials* **2010**, *31*, 7124−7131.
(42) Greish, K. *Methods Mol. Biol.* **2010**, *624*, 25−37.
(43) Sahoo, B.; Devi, K. S. P.; Banerjee, R.; Maiti, T. K.; Pramanik, P.; Dhara, D. *ACS Appl. Mater. Interfaces* **2013**, *5*, 3884−3893.
(44) Pietroiusti, A.; Campagnolo, L.; Fadeel, B. *Small* **2013**, *9*, 1557−1572.
(45) Yang, R.; Zhang, S.; Kong, D.; Gao, X.; Zhao, Y.; Wang, Z. *Pharm. Res.* **2012**, *29*, 3512−3525.
(46) Tang, Y.; Sun, G.; Cai, J.; Yang, P. *Anal. Methods* **2013**, *5*, 4602−4607.